Journal of Magnetic Resonance 305 (2019) 131–137

Contents lists available at ScienceDirect

Journal of Magnetic Resonance

journal homepage: www.elsevier.com/locate/jmr

Line narrowing in ^{1}H NMR of powdered organic solids with TOP-CT-MAS experiments at ultra-fast MAS

Federico M. Paruzzo, Brennan J. Walder, Lyndon Emsley *

Institut des Sciences et Ingénierie Chimiques, École Polytechnique Fédérale de Lausanne (EPFL), 1015 Lausanne, Switzerland

ARTICLE INFO

Article history:
Received 16 May 2019
Revised 25 June 2019
Accepted 26 June 2019
Available online 27 June 2019

Keywords:
Solid-state NMR
Ultra-fast MAS
^{1}H spectra
Constant time
Homonuclear dipolar decoupling

ABSTRACT

The residual broadening observed in ^{1}H spectra of rigid organic solids at natural abundance under 111 kHz magic angle spinning (MAS) is typically a few hundred Hertz. Here we show that refocusable and non-refocusable interactions contribute roughly equally to this residual at high-fields (21.14 T), and suggest that the removal of the non-refocusable part will produce significant increase in spectral resolution. To this end, we demonstrate an experiment for the indirect acquisition of constant-time experiments at ultra-fast MAS (CT-MAS) which verifies this hypothesis. The combination of this experiment with the two-dimensional one pulse (TOP) transformation reduces the experimental time to a fraction of the original cost while retaining the narrowing effects. Results obtained with TOP-CT-MAS at 111 kHz MAS on a sample of β-AspAla yield up to 30% higher resolution spectra than the equivalent one-pulse experiment, in less than 10 min.

1. Introduction

^{1}H is often considered a perfect nucleus for nuclear magnetic resonance (NMR): it is ubiquitous in chemistry, it has the highest gyromagnetic ratio of all the stable nuclei and nearly 100% natural isotopic abundance. However, this ensemble of qualities is not sufficient to guarantee success in solid-state NMR. Indeed, the use of ^{1}H is very limited in solids, where spectra of nuclei such as carbon-13, phosphorus-31 or silicon-29 are more common. This is mainly due to the line-broadening induced by strong ^{1}H homonuclear dipolar couplings – of the order of a few tens of kHz in organic solids – which leads to poor resolution in ^{1}H solid-state NMR. (In contrast, in liquid-state NMR rapid molecular tumbling largely averages dipolar couplings to zero, leading to very high-resolution spectra).

^{1}H spectral resolution in solids can be improved dramatically by magic angle spinning (MAS) [1,2]. Due to the strength of the homonuclear dipolar coupling, and due to the fact that it is a homogeneous interaction in the nomenclature of Maricq and Waugh [3], low to moderate spinning regimes (say <30 kHz MAS rates) lead, in general, to ^{1}H NMR spectra with line narrowing by factor ∼40–50, but this is not sufficient to alleviate the resolution problem (see Fig. 1a) [4–7]. Further decoupling can be achieved with the so-called combined rotation and multi-pulse spectroscopy (CRAMPS) approaches [8], which involve the simultaneous application of MAS and pulse sequences designed to remove homonuclear dipolar couplings while retaining isotropic chemical shifts [9–18]. This approach yields the best resolution available today for spinning rates up to ∼65 kHz, yielding linewidths in rigid organic solids on the order of 400 Hz [19,20]. These approaches have enabled a number of methods to characterise structure and dynamics in powdered solids [21–33]. However, the application of high-power decoupling for several milliseconds is a severe drawback as it is experimentally complex, technically demanding, and limits the maximum achievable resolution and sensitivity.

The recent introduction of probes capable of spinning samples up to 111 kHz [34,35] made the acquisition of reasonably high-resolution solid-state ^{1}H NMR spectra possible with MAS alone, as shown in Fig. 1b with the ^{1}H 111 kHz MAS spectrum of β-AspAla. With measured ^{1}H linewidths of about 250/300 Hz (≈0.3 ppm on a 900 MHz spectrometer), the spectral resolution is comparable to that obtained using state-of-the-art CRAMPS methods at lower MAS frequencies [16,17,20,36]. Despite the good resolution, the residual line broadening (which is estimated to be roughly 1% of the original broadening for organic solids in static conditions) still limits the use of ^{1}H NMR in the solid state, especially for complex systems.

Here, we develop a new experiment to further improve the resolution at ultra-fast MAS. Developing on the idea proposed by Lesage et al. [37] for CRAMPS spectra, we make use of constant-time acquisition in the indirect dimension of a 2D experiment to obtain spectra in which non-refocusable broadening is removed. We show results obtained on a sample of powdered microcrystalline β-AspAla, where spectral resolution is increased by up to 40% compared to one-pulse

* Corresponding author.
E-mail address: lyndon.emsley@epfl.ch (L. Emsley).

https://doi.org/10.1016/j.jmr.2019.06.015
1090-7807/

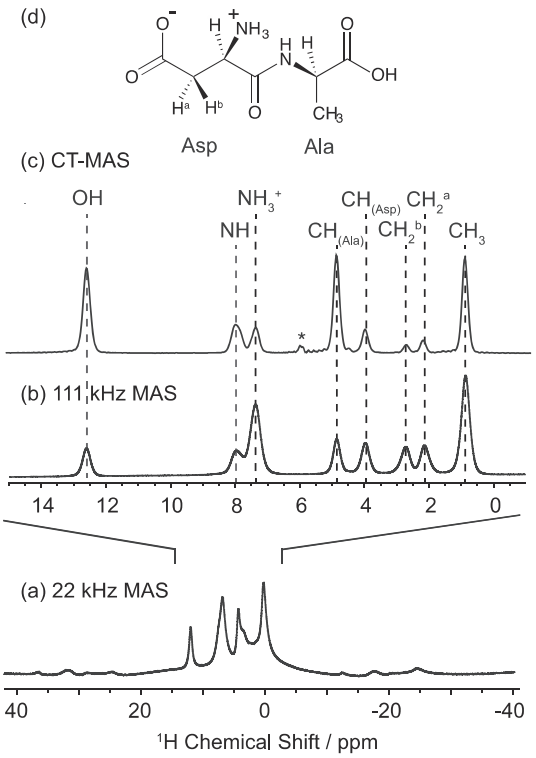

Fig. 1. (a–c) 1D ^{1}H spectra of powdered β-AspAla. (a and b) MAS spectra at 22 (a) and 111 (b) kHz MAS rates. (c) 111 kHz CT-MAS spectrum. Spectra (a–c) were acquired at 900 MHz using a one-pulse acquisition sequence (a and b) and the sequence of Fig. 2b (c). (d) Chemical formula of β-AspAla.

acquisition. Since the indirectly acquired spectrum is conventionally acquired point-by-point, however, obtaining high-resolution constant-time spectra from CT-MAS can require very long experiment times. Strategies utilizing spectral aliasing [38,39], non-uniform sampling [40], or covariance processing [41] are means of enhancing the resolution and information of such spectra in a time effective manner and are being actively developed.

In a unique alternative approach, Davis et al. demonstrated that the spectral windows of the direct and indirectly acquired dimensions in the 2D PASS experiment for sideband separation in rotating solids can be effectively swapped by the action of an affine transformation on the 2D dataset [42]. This allowed the indirectly detected signals to inherit the large spectral window of the directly acquired dimension. This method of transferring spectral windows by affine transformation of uniformly sampled data was referred to as TOP processing and was later shown to generalize to other sideband separation experiments [43,44]. Here we demonstrate that TOP processing is not specific to this class of solid-state NMR experiment but is applicable to any case where two interactions coevolve in the directly acquired signal and evolve independently along other coordinates in the 2D plane. We do this by showing how the TOP transformation permits an unaliased ^{1}H CT-MAS spectrum to be recovered from an indirect dimension that is severely undersampled with respect to the Nyquist rate of the ^{1}H shift spectrum. This approach improves the economy of the CT-MAS experiment by one to two orders of magnitude, leading to peaks up to 30% narrower than in the one-pulse experiment, acquired in less than 10 min.

2. Methods

2.1. NMR

Experiments were performed on a Bruker 900 US^2 wide-bore Avance Neo NMR spectrometer operating at a transmitter frequency 900.1448 MHz for ^{1}H, equipped with a H/C/N 0.7 mm CPMAS probe. All spectra were recorded using a rotor spinning rate (ν_r) of 111 kHz, with the only exception being the spectra of Fig. 1a which was recorded with ν_r = 22 kHz. A sample of powdered β-AspAla ((2S)-2-amino-3-{[(1S)-1-carboxyethyl]carbamoyl}propanoic acid, purity > 99%) was purchased from Bachem and used for all experiments without further recrystallization.

The transverse dephasing times (T_2') were measured using the Hahn echo sequence [45], shown in Fig. 2a. The measurement was done through a pseudo 2D experiment, based on the acquisition of a series of 1D MAS ^{1}H spectra where the time τ of decoupling was systematically increased in a multiple of the rotor period (τ_r). The dephasing curve was then obtained by plotting the area under each resonance as a function of the dephasing time (2τ). T_2' values were then extracted by fitting the dephasing curve to an exponential decay ($S(2\tau) = a * \exp(-2\tau/T_2')$).

Fig. 2b shows the pulse sequence used for the acquisition of constant-time MAS (CT-MAS) experiments. The initial $\pi/2$ pulse is followed by a $\tau_1 - \pi - \tau_2$ block (t_1 dimension), then a z-filter is applied before direct ^{1}H detection in t_2. During the experiment, the total time T of the block $\tau_1 - \pi - \tau_2$ is kept constant. The evolution of the magnetization during t_1 is induced by concomitantly increasing τ_1 in a multiple of the rotor period, while τ_2 is decreased. During t_1 evolution, the π pulse is incrementally moved from the center (where $t_1 = 0$) to the end of the T period. Analogously to the CT-CRAMPS [37] experiment, this experiment makes use of hypercomplex acquisition in the manner of States, Haberkorn, and Ruben [46] to acquire the negative t_1 quadrant. The result is a two-dimensional dataset with the ordinary MAS ^{1}H spectrum in ω_2 and the ^{1}H spectrum free of non-refocusable broadening (the homogeneous interactions) in ω_1 [37].

All CT-MAS experiments were acquired with 256 points in the indirect dimension. The indirect sampling intervals (Δt_1) were 0.036 ms, 0.054 ms, 0.072 ms, and 0.144 ms respectively for the experiments with constant time intervals of T = 4.6 ms, 6.9 ms, 9.2 ms, and 18.5 ms. Note that the increment used for T = 18.5 ms corresponds to a 7 kHz window, which leads to aliasing of the ^{1}H spectrum. The 1D spectrum shown was reconstructed from the 2D dataset by merging the 1D spectra obtained summing the signals in the columns between 0.25 and 2.38 ppm, 2.39 and 9.87 ppm, 9.88 and 13.80 ppm.

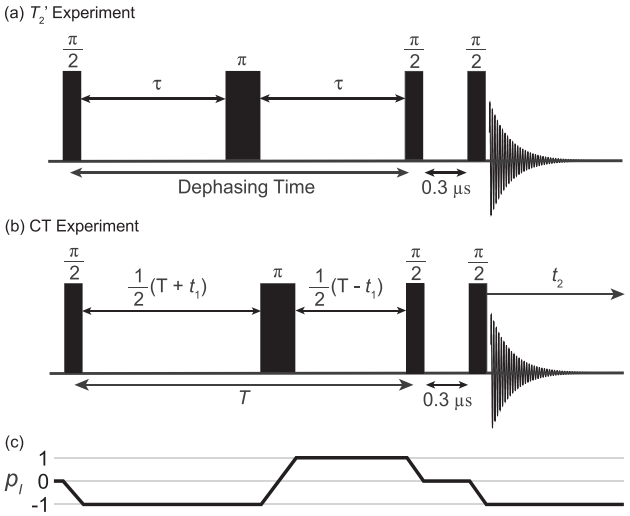

Fig. 2. (a and b) Pulse sequences for: (a) measurement of the transverse dephasing time (T_2'), (b) CT-MAS experiments. (c) Symmetry pathway selected by phase cycling for the TOP-CT-MAS implementation of the pulse sequence in panel (b). Detailed pulse program, experimental details for the spectra recorded, and the phase cycle are given in the experimental section and the ESI.

Formally, the TOP-CT-MAS experiments are implemented with a pulse sequence identical to the sequence used in the CT-MAS experiment, shown in Fig. 2b. Each TOP-CT-MAS experiment was run with an indirect sampling interval of $\Delta t_1 = 1.081$ ms. For the experiments at constant time intervals of $T = 4.9$ ms, 9.8 ms, and 17.8 ms, there were 8, 16, and 32 points in the indirect dimension, respectively. Application of the TOP transformation is facilitated by phase cycling for the symmetry pathway shown in Fig. 2c and running the π pulse from the beginning to the end of the constant time interval. This results in direct, phase-sensitive acquisition of the negative t_1 signal quadrant to permit absorption mode lineshapes without resorting to hypercomplex acquisition [46,47], as chosen for the conventional CT-MAS implementation.

^{1}H chemical shifts were referenced to the CH_3 resonance observed for β-AspAla at 0.86 ppm with respect to the signal for neat tetramethylsilane (TMS) [16]. All linewidths reported are full width at half maximum linewidths. The processing of the spectra was done either using the Bruker program TopSpin 3.5 for 1D and 2D CT-MAS experiments or using RMN 1.8.4 for 2D TOP-CT-MAS [48]. The post-processing procedures for the T_2' measurements (extraction of 1D spectra, evaluation of the area under each peak, fitting and extraction of T_2' value), as well as the extraction of the experimental ^{1}H linewidths for all spectra, were done in MATLAB using home-written scripts. Full details of acquisition parameters, phase cycles and pulse sequences are given in SI.

2.2. TOP-CT-MAS processing

Fig. 3 gives a visual outline of the TOP processing algorithm applied to simulated CT-MAS data. The two-dimensional dataset as acquired separates the constant-time signal evolution, which proceeds along the vertical ϵ_A axis (which corresponds to t_1 in the pulse sequence of Fig. 2b), from the decay due to non-refocusable signal components, which evolves purely along the diagonal axis $t = -\epsilon_A$. This coordinate is designated ϵ_B. Along the horizontal t axis (which corresponds to t_2 in the pulse sequence of Fig. 2b), the directly detected MAS spectrum evolves with both refocusable and non-refocusable contributions to its linewidth. This structure, where separated interactions evolve along nonorthogonal dimensions and coevolve in the directly acquired signal, is like that of the 2D PASS experiment, where the use of the TOP transformation to effectively swap the sampling intervals of the direct and indirectly acquired dimensions was first described by Davis et al. [42]. Indeed, we can achieve the same effect in the CT-MAS experiment using the affine transformation:

$$\begin{bmatrix} t_B \\ t_A \end{bmatrix} = \underbrace{\begin{bmatrix} 1 & -1 \\ 0 & 1 \end{bmatrix}}_{K_{t_B}} \underbrace{\begin{bmatrix} 1 & 0 \\ 1 & 1 \end{bmatrix}}_{K_t} \begin{bmatrix} \in_A \\ t \end{bmatrix} = \begin{bmatrix} 0 & -1 \\ 1 & 1 \end{bmatrix} \begin{bmatrix} \in_A \\ t \end{bmatrix}. \quad (1)$$

The strategy is to actively transform the data such that the two interaction dimensions, ϵ_A and ϵ_B, lie along the horizontal and vertical dimensions of the coordinate grid. The new respective coordinates, t_A and t_B, inherit the sampling properties of the grid axis onto which they are transformed. The first shear, represented by the matrix $\boldsymbol{K}_t$, maps the ϵ_B coordinate onto the vertical axis of the grid. Because only signal amplitude changes along this coordinate, the spectrum is centered about zero with a linewidth that reflects the non-refocusable linewidth of the MAS spectrum, suitable for the narrow spectral window of the vertical dimension. This is evident in the spectrum corresponding to the vertical cross-section of the 2D dataset after the first shear shown in Fig. 3b. After the second shear, represented by the matrix $\boldsymbol{K}_{t_B}$, the original ϵ_A axis is mapped onto the horizontal axis of the grid. In practice, the sam-

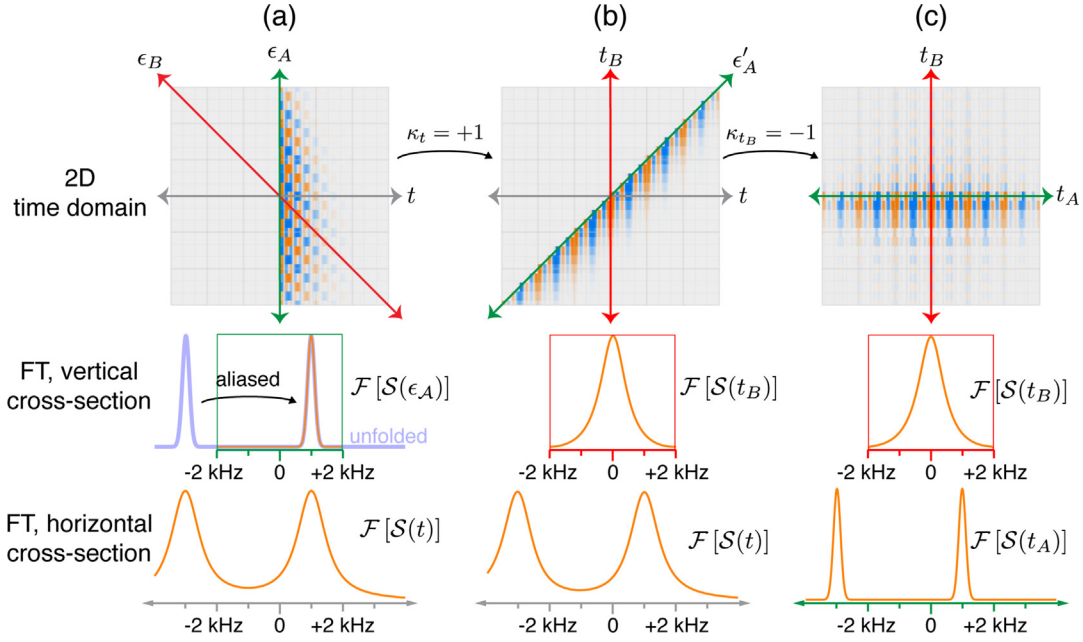

Fig. 3. The TOP double shear transformation of a simulated signal comprised of two peaks. (a) Representation of the undersampled CT-MAS dataset. The constant-time shift evolution (interaction 'A') evolves along the vertical axis designated by the time coordinate ϵ_A (green) while the decay from non-refocusable components (interaction 'B') evolves along the line $t = -\epsilon_A$, designated by the time coordinate ϵ_B (red). Fourier transform of the signal along ϵ_A yields an aliased constant-time shift spectrum where the peak at −3 kHz from the full spectrum (overlaid in blue) is aliased into the window, directly onto the peak at +1 kHz. The directly acquired t coordinate (horizontal, gray), having a much higher bandwidth, contains the unaliased but broadened spectrum. (b) After the first active shearing transformation parallel to t (shear factor $\kappa_t = +1$), the signal along ϵ_A is shifted onto the vertical axis, along the coordinate designated t_B, while the ϵ_A coordinate now runs parallel to the line $t = +t_B$. Fourier transform of the signal along t_B yields the lineshape due to non-refocusable components, whereas the spectrum along t is unchanged. (c) The second active shearing transformation, parallel to t_B (shear factor $\kappa_{t_B} = -1$), shifts the signal along the ϵ'_A axis onto the horizontal axis, along the coordinate designated t_A. Fourier transform of the signal along t_A presents the unaliased constant-time shift spectrum. Note the coordinate grid itself is unaffected by the active transformations. (For interpretation of the references to colour in this figure legend, the reader is referred to the web version of this article.)

pling interval of this dimension can be set very small, and the originally undersampled spectrum is unaliased as the correspondingly large bandwidth of the horizontal axis is inherited, as can be seen in Fig. 3c.

In most useful circumstances, applying the TOP transformation matrix $\boldsymbol{K}_{t_B}\boldsymbol{K}_t$ directly to the data vectors will map most of them off the grid nodes. Therefore, interpolation back onto the sampling grid is required. This is conveniently achieved by applying the shearing transformations as their operational equivalents in the mixed time-frequency domain according to the Fourier Affine Theorem. We carried this out using the macOS application RMN, as described in the TOP-CT-MAS processing walkthrough given in the ESI.

Not all linearly sampled 2D signals can have their sampling intervals effectively swapped by TOP processing. Qualifying conditions are discussed in Section 3.3.

3. Results and discussion

3.1. Lineshape contributions

Fig. 4a shows the dephasing curves of the eight ^{1}H resonances of β-AspAla, acquired using the sequence of Fig. 2a. As described above, by fitting these curves to an exponential decay it is possible to obtain the corresponding T_2' values, which by definition corresponds to the residual broadening induced by non-refocusable interactions, such as homonuclear dipolar coupling [49]. From these curves, we can estimate that non-refocusable interactions contribute up to about a third of the measured line broadening observed in a one-pulse acquire experiment of the type shown in Fig. 1b, as it is shown in Fig. 4b. This is in line with previous observations under both CRAMPS and fast MAS [7,17,37]. Removing this contribution would in principle lead to a significant improvement in the spectral resolution, without affecting chemical shift information (which would be refocused by the application of the π pulse).

3.2. CT-MAS

The constant-time (CT) principle [50–55] has already proven to be an effective way to remove broadening due to non-refocusable interactions from ^{1}H spectra in the solid-state. This idea was introduced by Lesage et al. with the CT-CRAMPS experiment [37]. They have shown that constant time acquisition in the indirect dimension of a 2D dataset leads to pure refocusable spectra, which have 2–3 times narrower resonances compared to CRAMPS experiments at 12.5 kHz MAS. In this experiment, the application of high power homonuclear decoupling was necessary to enter the weak coupling regime where the CT principle is likely to be most valid.

Today, with the line narrowing achieved using the highest MAS rates available, we can make use of the CT principle with MAS alone [56]. We can then obtain pure refocusable spectra by using the CT-MAS experiment, shown in Fig. 2b. Fig. 5a shows the 111 kHz CT-MAS spectra of β-AspAla acquired using constant time periods (T) ranging from 4.6 to 18.5 ms.

When compared with the one-pulse ^{1}H spectra recorded at 111 kHz MAS (Fig. 1b), all spectra show a significant improvement in the spectral resolution. Line narrowing is already achieved at T = 4.6 ms, despite truncation of the signal due to the short CT period. In this spectrum the experimental linewidths are on average 17% narrower than the ones obtained with the one-pulse experiment. The CH_2 resonances give the highest gain in resolution with 30% narrower linewidths (from about 300 to 210 Hz). On the other

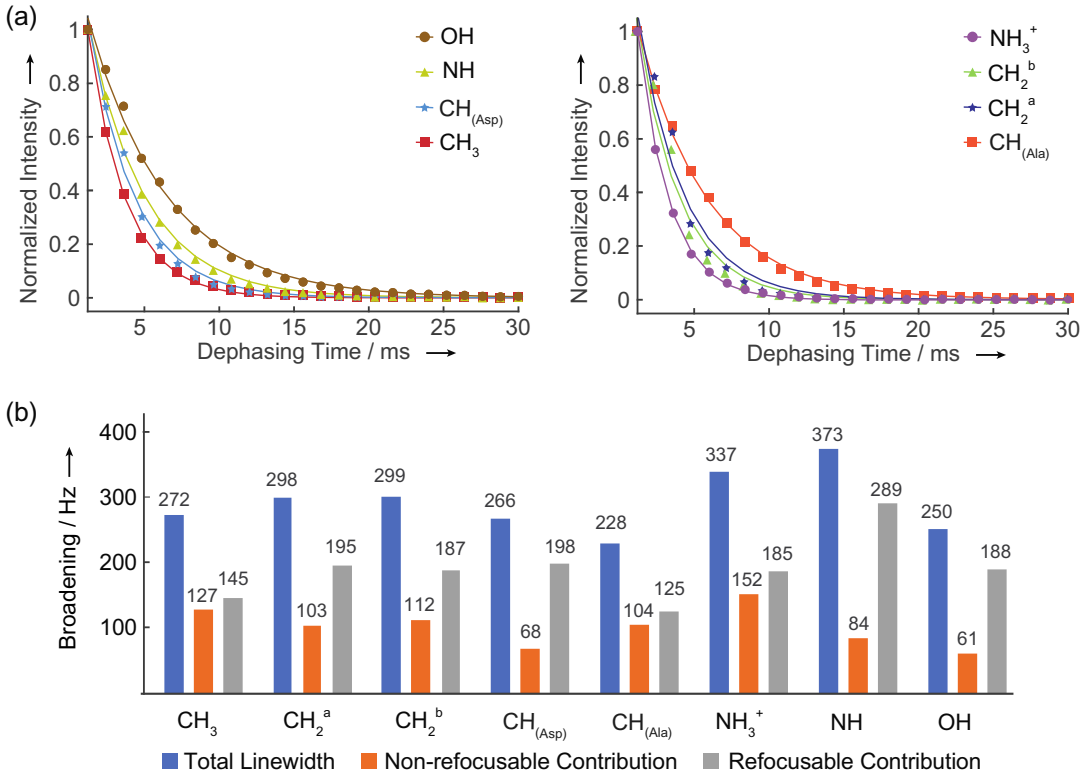

Fig. 4. (a) Dephasing curves for the ^{1}H resonances of powdered β-AspAla recorded using the pulse sequence of Fig. 2a. Each curve is normalized with respect to the corresponding highest intensity point. (b) Histogram of the contributions to the line broadening of the resonances of powdered β-AspAla at 111 kHz MAS. The total linewidth (in blue) is the linewidth measured from the experimental spectrum of Fig. 1b, the contributions of non-refocusable interactions (in orange) were calculated from the T_2' values ($\Delta_{\text{homo}} = 1/\pi T_2'$) and the contributions of the refocusable interactions (in grey) were obtained from the difference between the total and non-refocusable broadenings. (For interpretation of the references to colour in this figure legend, the reader is referred to the web version of this article.)

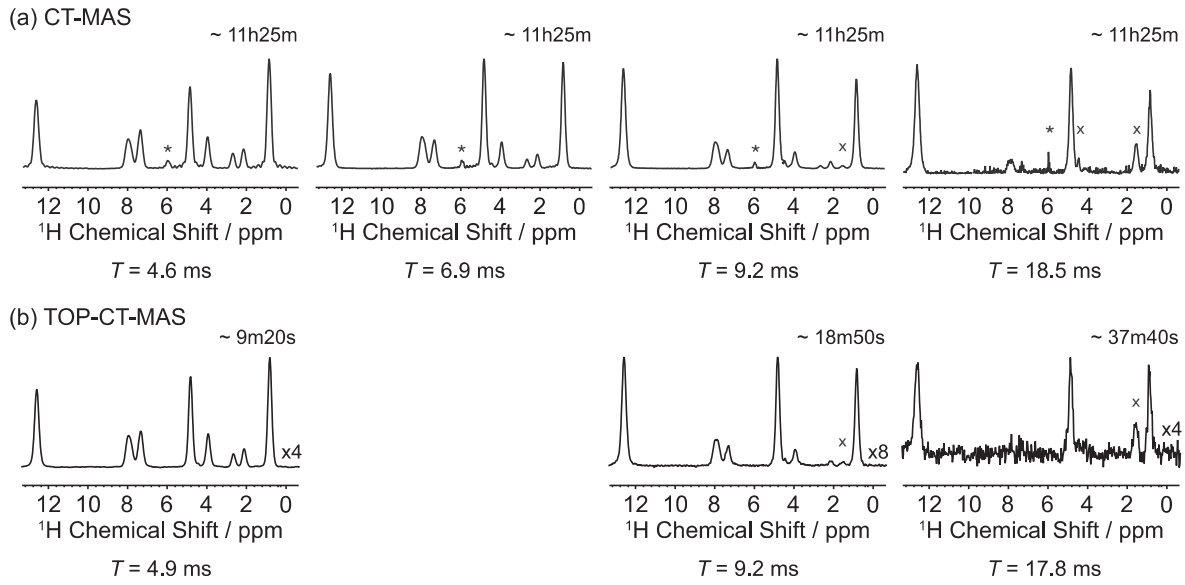

Fig. 5. Comparison between different 1D ^{1}H spectra of β-AspAla acquired with (a) the CT-MAS experiment and (b) the TOP-CT-MAS experiments. CT-MAS spectra were acquired using constant-time periods (T) of 4.6, 6.9, 9.2 and 18.5 ms, while TOP-CT-MAS using T of 4.9, 9.2 and 17.8 ms. CT-MAS spectra are the vertical projection of the two-dimensional experiments, while TOP-CT-MAS spectra are the extraction of the central row. The transmitter peak is indicated with an asterisk, which is better suppressed in the TOP-CT-MAS experiments due to a superior phase cycle (see ESI). Peaks due to impurities are marked with an x. On the top-right corner of each spectrum is reported the corresponding acquisition time for comparison.

hand, nearly no line narrowing effect was observed for the OH resonance, probably due to the presence of dynamics or exchange.

The spectral resolution can be further improved by increasing the T value. This, however, comes at the expense of sensitivity, which decreases when increasing T at a rate that depends on the T_2'. The dependence on T_2' also affects the relative signal intensities in the CT-MAS spectra, which become different to those obtained with ordinary MAS experiments (Fig. 1b and c). The resonances with longer T_2' will decay at a slower rate, resulting in higher relative intensities. At T = 6.8 ms the resonances are on average 23% sharper than in the one-pulse experiment, with each resonance being at least 8% narrower than the corresponding peak in the one-pulse spectrum. T = 6.8 ms is also short enough to allow the observation of all the ^{1}H resonances in our sample. Further increase of T still provides additional line-narrowing effects, but decreases the sensitivity down to a point where some of the resonances are no longer visible. At the longest CT period we used (T = 18.5 ms) only three peaks remain: the CH_3, $CH_{(Ala)}$ and the OH. Of these, the CH_3 shows a remarkable improvement in resolution, with a linewidth of 171 Hz, about 37% smaller than the 272 Hz observed in the one-pulse experiment. The improvement for the other two resonances is less: 16% for the $CH_{(Ala)}$ and only 3% for the OH. Note that in the spectra there are also two additional peaks at 1.6 and 4.5 ppm (which appear already at T = 9.2 ms). These might be due to impurities with long T_2'which are not observed in the one-pulse experiment. The full set of measured linewidths for these experiments is given in SI.

At this point, it is important to underline that in this experiment the line narrowing effect is not only due to the CT effect. As shown previously for the CT-CRAMPS experiment [37], part of the reduction in linewidth is due to the presence of the long echo which delays signal acquisition. During this delay the signal of protons in the more strongly coupled average orientations will dephase preferentially, leaving relatively stronger signals from protons in more weakly coupled average orientations, leading to line narrowing.

This is supported by the fact that in these spectra we observe significant line narrowing both in ω_1 and in ω_2 (where there is no CT effect). In particular, we observed that at 111 kHz MAS rate the narrowing due to the CT effect contributes only 35% of the total line narrowing. This is in contrast with what has been observed for CT-CRAMPS experiments where most of the narrowing was induced by the CT acquisition.

3.3. TOP-CT-MAS

The most significant difference between conventional CT-MAS and the TOP-CT-MAS implementation is that the indirect dimension of the latter is sampled at 0.925 kHz, well below the Nyquist rate of the ^{1}H chemical shift spectrum (about 12 kHz for β-AspAla at 21.14 T). Because of the correspondingly large indirect sampling interval (1.081 ms), the entire constant-time signal envelope can be collected with far fewer discrete samples than the conventional approach, making the TOP-CT-MAS implementation potentially far more economical in terms of experiment time. The obvious disadvantage is that Fourier transform of the indirect dimension, as acquired, presents a useless ^{1}H shift spectrum because of severe spectral aliasing resulting from the undersampling.

The affine transformation specified by Eq. (1) nullifies this disadvantage by reconstructing the unaliased, high-resolution constant-time ^{1}H spectrum in the large spectral window of the directly acquired dimension from a CT-MAS experiment with an undersampled ϵ_A coordinate. The sampling rate of the indirect dimension using the TOP transformation needs only to be small enough to accommodate the frequency components which evolve along the vertical grid axis *after* transformation of the dataset. This is controlled by the design of the experiment and processing protocol. Here, the TOP transformation maps the residual non-refocusable broadening onto the vertical axis. For each site in our β-AspAla sample linewidths are no greater than 160 Hz, as shown in Fig. 4b. A sampling rate of less than 1 kHz suffices for sampling the ϵ_A dimension in the TOP approach, for a potential reduction in experiment time by one to two orders of magnitude when TOP processing principles are leveraged. Note that if the indirect sampling rate dimension is so low that the t_B coordinate is undersampled, the TOP transformation will introduce sidebands into the spectrum along the t_A coordinate at integer multiples of the indirect sam-

pling rate. Generally, the decay of the non-refocusable contributions is exponential, so these sidebands manifest more strongly among the undesired long-tailed dispersive signal components, as shown in Fig. S1 in the ESI. This improves the robustness of the approach in the face of a poor estimation of an appropriate indirect sampling interval.

In Fig. 5a that has an indirect sampling rate of 27.75 kHz, conventional CT-MAS experiments took more than 11 h to complete. Note that an unnecessarily long 32-step phase cycle was used, but even if the conventional CT-MAS experiments had used the 14-step phase cycle to select the symmetry pathway in Fig. 2c directly, each experiment would still have taken nearly six hours to complete. In Fig. 5b, we see comparable high-resolution constant-time ^{1}H spectra constructed from undersampled ϵ_A coordinates using the TOP approach. When T = 4.9 ms, just eight points in the indirect dimension are enough to obtain the narrowed proton spectrum, in an experiment lasting less than ten minutes. Furthermore, in the TOP-CT-MAS experiments with constant time intervals of 4.9 ms and 17.8 ms no loss in signal-to-noise per unit time was observed when compared to the CT-MAS experiment at 4.6 and 18.3 ms, while the experiment with T = 9.2 ms shows about 30% less sensitivity when the TOP transformation is applied. Here, the overall reduction in experiment time for experiments at comparable T normalised to the number of scans was between a factor 8 and 32 using the TOP implementation.

Undersampling the indirect dimension of the CT-MAS experiment does not quantitatively affect the line width measurements when TOP processing is used. We show in the ESI that linewidths in the constant-time ^{1}H spectra are comparable between conventional CT-MAS and the TOP-CT-MAS implementation. In fact, we see from Fig. 3c that the final 2D TOP-CT-MAS dataset correlates evolution along the t_A and t_B coordinates along orthogonal dimensions. We can therefore measure site-specific non-refocusable contributions to linewidths in the dimension orthogonal to the constant-time ^{1}H spectrum. We also show in the SI that the non-refocusable contributions determined from the TOP-CT-MAS experiments are comparable to those determined from the T_2' experiments shown in Fig. 4b.

At first sight, it might appear that the TOP transformation circumvent a seemingly fundamental limitation on the bandwidth of linearly sampled signals. This is not the case. First, the Nyquist criterion should only be expected to apply strictly to directly acquired signals, since acquisition actually proceeds along the indirect dimension by concatenation of separate experiments. More importantly, however, is that interactions ‘A’ and ‘B’ coevolve in the directly acquired signal. Signals acquired along the indirect dimension need then only supply the information necessary to allow deconvolution of the two interactions. When, as in 2D PASS and CT-MAS, the experiment is designed such that interactions ‘A’ and ‘B’ evolve independently along oblique coordinates in the initial 2D coordinate system, an affine transformation exists for separating and correlating them along orthogonal dimensions in the final 2D coordinate system. For the classes of 2D experiments that do not possess this property, however, TOP processing cannot effectively swap the direct and indirect sampling intervals. This is true, for example, of the two shift spectra axes in a 2D heteronuclear correlation experiment.

Finally, it is worth noting that when using the strategy of direct pathway selection, use of the z-filter with hypercomplex acquisition is unnecessary to obtain pure absorption mode lineshapes provided that the pulse is moved from the beginning to the end of the constant-time interval. Thus, only the first two pulses are necessary for the minimal CT-MAS experiment, allowing a phase cycle with as few as 3 steps. If sensitivity is not a limiting factor, this would permit acquisition of constant time ^{1}H spectra in less than two minutes.

4. Conclusions

In summary, we find that the non-refocusable contribution to residual line broadening at 111 kHz MAS in β-AspAla is around 30–40%, from T_2 measurements. We show that this contribution can be removed in 2D constant time experiments, leading to linewidths up to 40% narrower than the one-pulse experiment. We observe that this narrowing due both to the CT effect, and the effect of the delayed acquisition due to the constant-time echo. Despite the line narrowing effect, this experiment requires long experimental times to obtain high-resolution in the indirect dimension. We overcome this drawback by adapting the experiment to the TOP transformation. The resulting TOP-CT-MAS experiment provides comparable results to the conventional CT-MAS experiment, but in a fraction of the experimental time. For β-AspAla we obtained ^{1}H spectra with up to a 30% improvement in resolution as compared to the one-pulse experiment, in less than 10 min.

Acknowledgments

We are grateful for financial support from Swiss National Science Foundation Grant Nos. 200021_160112 and 200020_178860.

Declaration of Competing Interest

There are no conflicts to declare.

Appendix A. Supplementary material

Supplementary data to this article can be found online at https://doi.org/10.1016/j.jmr.2019.06.015.

References

[1] I. Lowe, Free induction decays of rotating solids, Phys. Rev. Lett. 2 (1959) 285.
[2] E.R. Andrew, A. Bradbury, R.G. Eades, Removal of dipolar broadening of nuclear magnetic resonance spectra of solids by specimen rotation, Nature 183 (1959) 1802–1803.
[3] M.M. Maricq, J.S. Waugh, NMR in rotating solids, J. Chem. Phys. 70 (1979) 3300.
[4] E. Brunner, D. Freude, B. Gerstein, H. Pfeifer, Residual linewidths of NMR spectra of spin-12 systems under magic-angle spinning, J. Magnet. Reson. (1969) 90 (1990) 90–99.
[5] M. Levitt, D. Raleigh, F. Creuzet, R. Griffin, Theory and simulations of homonuclear spin pair systems in rotating solids, J. Chem. Phys. 92 (1990) 6347–6364.
[6] V.E. Zorin, S.P. Brown, P. Hodgkinson, Origins of linewidth in H 1 magic-angle spinning NMR, J. Chem. Phys. 125 (2006) 144508.
[7] U. Sternberg, R. Witter, I. Kuprov, J.M. Lamley, A. Oss, J.R. Lewandowski, A. Samoson, 1H line width dependence on MAS speed in solid state NMR–comparison of experiment and simulation, J. Magnet. Reson. 291 (2018) 32–39.
[8] B.C. Gerstein, R.G. Pembleton, R.C. Wilson, L.M. Ryan, High resolution NMR in randomly oriented solids with homonuclear dipolar broadening: combined multiple pulse NMR and magic angle spinning, J. Chem. Phys. 66 (1977) 361.
[9] M. Lee, W.I. Goldburg, Nuclear-magnetic-resonance line narrowing by a rotating rf field, Phys. Rev. 140 (1965) A1261–A1271.
[10] J.S. Waugh, L.M. Huber, U. Haeberlen, Approach to high-resolution nmr in solids, Phys. Rev. Lett. 20 (1968) 180–182.
[11] P. Mansfield, Symmetrized pulse sequences in high resolution NMR in solids, J. Phys. C: Solid State Phys. 4 (1971) 1444.
[12] D.P. Burum, W.K. Rhim, Analysis of multiple pulse NMR in solids III, J. Chem. Phys. 71 (1979) 944.
[13] A. Bielecki, A. Kolbert, M. Levitt, Frequency-switched pulse sequences: homonuclear decoupling and dilute spin NMR in solids, Chem. Phys. Lett. 155 (1989) 341–346.
[14] E. Vinogradov, P. Madhu, S. Vega, High-resolution proton solid-state NMR spectroscopy by phase-modulated Lee-Goldburg experiment, Chem. Phys. Lett. 314 (1999) 443–450.
[15] D. Sakellariou, A. Lesage, P. Hodgkinson, L. Emsley, Homonuclear dipolar decoupling in solid-state NMR using continuous phase modulation, Chem. Phys. Lett. 319 (2000) 253–260.
[16] B. Elena, G. de Paëpe, L. Emsley, Direct spectral optimisation of proton–proton homonuclear dipolar decoupling in solid-state NMR, Chem. Phys. Lett. 398 (2004) 532–538.

[17] M.E. Halse, L. Emsley, Improved phase-modulated homonuclear dipolar decoupling for solid-state NMR spectroscopy from symmetry considerations, J. Phys. Chem. A 117 (2013) 5280–5290.
[18] W.K. Rhim, Analysis of multiple pulse NMR in solids, J. Chem. Phys. 59 (1973) 3740.
[19] M. Leskes, S. Steuernagel, D. Schneider, P. Madhu, S. Vega, Homonuclear dipolar decoupling at magic-angle spinning frequencies up to 65 kHz in solid-state nuclear magnetic resonance, Chem. Phys. Lett. (2008) 95–99.
[20] E. Salager, J.-N. Dumez, R.S. Stein, S. Steuernagel, A. Lesage, B. Elena-Herrmann, L. Emsley, Homonuclear dipolar decoupling with very large scaling factors for high-resolution ultrafast magic angle spinning 1H solid-state NMR spectroscopy, Chem. Phys. Lett. 498 (2010) 214–220.
[21] S.P. Brown, H.W. Spiess, Advanced solid-state NMR methods for the elucidation of structure and dynamics of molecular, macromolecular, and supramolecular systems, Chem. Rev. 101 (2001) 4125–4156.
[22] C. Ochsenfeld, S.P. Brown, I. Schnell, J. Gauss, H.W. Spiess, Structure assignment in the solid state by the coupling of quantum chemical calculations with NMR experiments: a columnar hexabenzocoronene derivative, J. Am. Chem. Soc. 123 (2001) 2597–2606.
[23] S.P. Brown, A. Lesage, B. Elena, L. Emsley, Probing proton−proton proximities in the solid state: high-resolution two-dimensional 1H–1H double-quantum CRAMPS NMR spectroscopy, J. Am. Chem. Soc. 126 (2004) 13230–13231.
[24] S.P. Brown, Recent advances in solid-state MAS NMR methodology for probing structure and dynamics in polymeric and supramolecular systems, Macromol. Rapid Commun. 30 (2009) 688–716.
[25] E. Salager, R.S. Stein, C.J. Pickard, B. Elena, L. Emsley, Powder NMR crystallography of thymol, Phys. Chem. Chem. Phys. 11 (2009) 2610–2621.
[26] D. Dudenko, A. Kiersnowski, J. Shu, W. Pisula, D. Sebastiani, H.W. Spiess, M.R. Hansen, A strategy for revealing the packing in semicrystalline Π-conjugated polymers: crystal structure of bulk poly-3-hexyl-thiophene (P3HT), Angew. Chem. Int. Ed. 51 (2012) 11068–11072.
[27] M. Baias, C.M. Widdifield, J.N. Dumez, H.P. Thompson, T.G. Cooper, E. Salager, S. Bassil, R.S. Stein, A. Lesage, G.M. Day, L. Emsley, Powder crystallography of pharmaceutical materials by combined crystal structure prediction and solid-state 1H NMR spectroscopy, Phys. Chem. Chem. Phys. 15 (2013) 8069–8080.
[28] S.R.M. Santos, J.O. Rocha, L. Mafra, NMR crystallography: toward chemical shift-driven crystal structure determination of the β-Lactam antibiotic amoxicillin trihydrate, Crystal Growth Des. 13 (2013) 2390–2395.
[29] J.A. Fernandes, M. Sardo, L. Mafra, D. Choquesillo-Lazarte, N. Masciocchi, X-ray and NMR crystallography studies of novel theophylline cocrystals prepared by liquid assisted grinding, Crystal Growth Des. 15 (2015) 3674–3683.
[30] P. Paluch, T. Pawlak, M. Oszajca, W. Lasocha, M.J. Potrzebowski, Fine refinement of solid state structure of racemic form of phospho-tyrosine employing NMR Crystallography approach, Solid State Nucl. Magnet. Reson. 65 (2015) 2–11.
[31] J. Leclaire, G. Poisson, F. Ziarelli, G. Pepe, F. Fotiadu, F.M. Paruzzo, A.J. Rossini, J.-N. Dumez, B. Elena-Herrmann, L. Emsley, Structure elucidation of a complex CO 2-based organic framework material by NMR crystallography, Chem. Sci. 7 (2016) 4379–4390.
[32] C.M. Widdifield, H. Robson, P. Hodgkinson, Furosemide's one little hydrogen atom: NMR crystallography structure verification of powdered molecular organics, Chem. Commun. 52 (2016) 6685–6688.
[33] M. Baias, J.N. Dumez, P.H. Svensson, S. Schantz, G.M. Day, L. Emsley, De novo determination of the crystal structure of a large drug molecule by crystal structure prediction-based powder NMR crystallography, J. Am. Chem. Soc. 135 (2013) 17501–17507.
[34] V. Agarwal, S. Penzel, K. Szekely, R. Cadalbert, E. Testori, A. Oss, J. Past, A. Samoson, M. Ernst, A. Böckmann, B.H. Meier, De Novo 3D structure determination from sub-milligram protein samples by solid-state 100 kHz MAS NMR spectroscopy, Angew. Chem. Int. Ed. 53 (2014) 12253–12256.
[35] Y. Nishiyama, M. Malon, Y. Ishii, A. Ramamoorthy, 3D 15 N/15 N/1 H chemical shift correlation experiment utilizing an RFDR-based 1 H/1 H mixing period at 100kHz MAS, J. Magnet. Reson. 244 (2014) 1–5.
[36] M.E. Halse, J. Schlagnitweit, L. Emsley, High-Resolution1H solid-state NMR spectroscopy using windowed LG4 homonuclear dipolar decoupling, Israel J. Chemi. 54 (2014) 136–146.
[37] A. Lesage, L. Duma, D. Sakellariou, L. Emsley, Improved resolution in proton NMR spectroscopy of powdered solids, J. Am. Chem. Soc. 123 (2001) 5747–5752.
[38] P. Schmieder, S. Zimmer, H. Kessler, Increased resolution in proton detected heteronuclear NMR experiments by folding in the hetero-dimension, Magnet. Reson. Chem. 29 (1991) 375–380.
[39] D. Jeannerat, Computer optimized spectral aliasing in the indirect dimension of 1H–13C heteronuclear 2D NMR experiments. A new algorithm and examples of applications to small molecules, J. Magnet. Reson. 186 (2007) 112–122.
[40] J.C. Hoch, M.W. Maciejewski, M. Mobli, A.D. Schuyler, A.S. Stern, Nonuniform sampling and maximum entropy reconstruction in multidimensional NMR, Acc. Chem. Res. 47 (2014) 708–717.
[41] R. Brüschweiler, F. Zhang, Covariance nuclear magnetic resonance spectroscopy, J. Chem. Phys. 120 (2004) 5253–5260.
[42] M.C. Davis, K.M. Shookman, J.D. Sillaman, P.J. Grandinetti, TOP-PASS: a processing algorithm to reduce 2D PASS acquisition time, J. Magnet. Reson. 210 (2011) 51–58.
[43] B.J. Walder, K.K. Dey, D.C. Kaseman, J.H. Baltisberger, P.J. Grandinetti, Sideband separation experiments in NMR with phase incremented echo train acquisition, J. Chem. Phys. 138 (2013) 174203.
[44] C.E. Avalos, B.J. Walder, J. Viger-Gravel, A. Magrez, L. Emsley, Chemical exchange at the ferroelectric phase transition of lead germanate revealed by solid state 207 Pb nuclear magnetic resonance, Phys. Chem. Chem. Phys. 21 (2019) 1100–1109.
[45] E.L. Hahn, Spin echoes, Phys. Rev. 80 (1950) 580.
[46] D. States, R. Haberkorn, D. Ruben, A two-dimensional nuclear Overhauser experiment with pure absorption phase in four quadrants, J. Magnet. Reson. (1969) 48 (1982) 286–292.
[47] P.J. Grandinetti, J.T. Ash, N.M. Trease, Symmetry pathways in solid-state NMR, Progr. Nucl. Magnet. Reson. Spectrosc. 59 (2011) 121.
[48] PhySy Lrd, RMN, Version 1.8 (www.physyapps.com, PhySy Ltd., Grand-view Heights, OH 43212).
[49] A. Lesage, M. Bardet, L. Emsley, Through-bond carbon-carbon connectivities in disordered solids by NMR, J. Am. Chem. Soc. 121 (1999) 10987–10993.
[50] A. Bax, A. Mehlkopf, J. Smidt, Absorption spectra from phase-modulated spin echoes, J. Magnet. Reson. (1969) 35 (1979) 373–377.
[51] A. Bax, R. Freeman, Investigation of complex networks of spin-spin coupling by two-dimensional NMR, J. Magnet. Reson. (1969) 44 (1981) 542–561.
[52] M. Rance, G. Wagner, O. Sørensen, K. Wüthrich, R. Ernst, Application of ω1-decoupled 2D correlation spectra to the study of proteins, J. Magnet. Reson. (1969) 59 (1984) 250–261.
[53] R. Powers, A.M. Gronenborn, G.M. Clore, A. Bax, Three-dimensional triple-resonance NMR of 13 C/15 N-enriched proteins using constant-time evolution, 1991.
[54] J. Santoro, G.C. King, A constant-time 2D overbodenhausen experiment for inverse correlation of isotopically enriched species, J. Magnet. Reson. (1969) 97 (1992) 202–207.
[55] G.W. Vuister, A. Bax, Resolution enhancement and spectral editing of uniformly 13C-enriched proteins by homonuclear broadband 13C decoupling, J. Magnet. Reson. (1969) 98 (1992) 428–435.
[56] H. Colaux, Y. Nishiyama, Resolution enhancement in proton double quantum magic-angle spinning spectra by constant-time acquisition, Solid State Nucl. Magnet. Reson. (2017).